Luminescence of $Cd_{0.7}Mn_{0.3}Te$ Crystals in Transverse Magnetic Field

R. Brazis[a,*], L. Barauskaitė[a], V. Ivanov[b] and M. Godlewski[b]

[a]Semiconductor Physics Institute, A. Goštauto g. 11, 01108 Vilnius, Lithuania
[b]Institute of Physics, Polish Academy of Sciences
al. Lotników 32/46, 02-668 Warszawa, Poland

(Received March 21, 2005; revised version December 6, 2005)

Photoluminescence of cleaved $Cd_{0.7}Mn_{0.3}Te$ crystals is studied at $T \approx 1.6$ K at the normal- and oblique (45°) incidence of the pumping Ar laser beam ($\lambda = 488$ nm) in magnetic fields $-7 \leq B \leq 7$ T in the Voigt geometry. At $B = 0$, photoluminescence maximum is found at 2.0819 eV at normal incidence (and backward emission) whereas the oblique incidence and emission shows photoluminescence maximum intensity at 2.0536 eV. The red shift of photoluminescence maximum position with the rise in B is observed and the results are found to be in good agreement with $sp-d$ exchange interaction model for the oblique incidence case. Backward emitted photoluminescence line is found to narrow from 26.2 to 23.5 meV with the rise in B from 0 to 7 T. Alloy disorder contribution exhibits opposite trend to broaden, as is calculated on the basis of the matrix of the energy gap dependence on x and B. Therefore the observed photoluminescence line narrowing is assigned to the suppression of magnetic fluctuation in magnetic field. A linear size of magnetic fluctuation is estimated to be about 1/5 of the free exciton diameter. Photoluminescence maximum position difference in the normal- and oblique incidence cases is assigned to polaritons.

PACS numbers: 75.50.Pp, 78.55.Et, 71.35.–y

1. Introduction

Modern directions of spintronics and magneto-nanophotonics have branched from the research on diluted magnetic semiconductors (DMS). Among these, $Cd_{1-x}Mn_xTe$ crystals have been used for testing exchange interaction between electron (hole) and substitution ion spins [1–6]. Mn^{2+} ion magnetic moment align-

*corresponding author; e-mail: brazis@pfi.lt

ment has been shown to enhance the effects of external magnetic field on electron states in conduction and valence bands giving rise to giant magnetooptical effects, e.g., the Faraday rotation or the Voigt birefringence [7–10]. Photoluminescence (PL) research [6, 11–14] is of special interest on the way to magnetically tunable lasers. The present work focuses on the crystals with the Mn atom mole fraction of $x = 0.3$ that is already large enough to bring the PL band to the visible light range. However, the mean magnetisation gradually reduces with the increase in Mn contents in the crystal bulk due to the antiferromagnetic pairing of the nearest Mn neighbours giving rise to the spin–glass phase [15]. Nevertheless, the antiferromagnetically non-paired Mn^{2+} concentration at surface is suggested to be higher than in the bulk [16, 17]. The possibility of alloy transformation to the ferromagnetic $CdMnTe_2$ compound opens when approaching to $x = 0.5$ [18]. Although such large deviations from the selected nominal value of $x = 0.3$ seem unlike, they challenge for the study of alloy disorder. It is competing with more flexible magnetisation disorder related to the subsystem of Mn atom spins. The mean size of magnetic fluctuation is deducible from the comparison of fluctuation theory to experimental PL linewidth [19, 20].

Three main photoluminescence bands have been observed in $Cd_{1-x}Mn_xTe$ crystals [6]. The first (labelled A) has been assigned to the free excitons. The second one (labelled B) has been reported to be in the vicinity of 2 eV independent of x, when $x > 0.4$ [6] and referred to Mn atom transitions from an excited to the ground state, although other authors [14] attributed the peak to impurities. The third band (labelled C) observed in the vicinity of 1.2 eV has been attributed to the transitions from the Mn ion excited state to the valence band top [6]. The B- and C-band assignment, position, and width are tentative, e.g., additional comparatively shallow levels have been introduced in order to explain the band broadening [21].

In the present work, we are interested in the exciton PL band A. Experiments on reflectivity modulation have shown the position of the band to be $E_A/\text{eV} = 1.586 + 1.501x$ at $T = 80$ K, and $E_A/\text{eV} = 1.595 + 1.592x$ at $T = 10$ K [15]. Assuming that E_A changes linearly with temperature we deduce from these two equations the temperature dependence of $E_A/\text{eV} = 2.0778 - 5.164 \times 10^{-4}T$ for $x = 0.3$. This gives the value of $E_A = 2.077$ eV at our planned experimental temperature $T = 1.6$ K. However, the Voigt birefringence data interpolation gives $E_A = 2.066$ eV [10]. The intermediate band-gap value of 2.071 eV is deducible from experimental formula $E/\text{eV} = 1.595 + 1.587x$ for $T = 1.8$ K [4]. Gaj and co-workers [2] have reported the free exciton energy of 2.087 eV in $Cd_{0.7}Mn_{0.3}Te$ at $T = 1.4$ K from reflectivity measurements. Direct PL measurements by Hayes and co-workers in $Cd_{0.7}Mn_{0.3}Te$ [13] have shown the value of $E_A = 2.073$ eV at $T = 1.8$ K and $B = 0$.

The physical parameter spread from 2.066 to 2.087 eV in nominally the same composition material is remarkable. One can suspect that the spread is a

message on different alloy disorder in samples grown at different conditions. Another possibility comes from the translation symmetry truncation at the crystal surface that is suggested to orient ion magnetic moments predominantly normal to the surface [22]. It is also very likely that the PL maximum position is related to exciton–photon coupling (polariton) effect [23]. Such coupled states need assistance of other quasi-particles (phonons, magnons [24]) for the energy and momentum conservation in the acts of photon emission in outer space [25]. These coupled states seem to manifest differently depending on whether the light excitation and emission is normal or oblique, as a result of different in-plane momentum rendered to electron–hole pairs by the excitation laser beam.

This work has been aimed at experimental survey of PL spectra at the normal- and oblique incidence (and emission) of photons in the same $Cd_{0.7}Mn_{0.3}Te$ crystal samples in the Voigt geometry. Experimental details are presented in Sect. 2, the results are described in Sect. 3 and compared in Sect. 4 to existing PL line and linewidth models.

2. Experiment

$Cd_{0.7}Mn_{0.3}Te$ crystals were grown using modified Bridgeman technique and the samples have been prepared by the crystal cleaving in order to have optically perfect surface. Let us note that PL is not observable from polished or degraded (contaminated) surface. An Oxford Spectromag^{4000} cryostat with the superconducting coils has been used for measurements in magnetic field up to 7 T on samples immersed in liquid He pumped down to the temperature of $T = 1.6{-}1.7$ K in order to avoid noise coming from the light scattering on boiling liquid He. The Ar laser line of $\hbar\omega = 2.54$ eV ($\lambda = 488$ nm) has been used for excitation, and the laser beam polarised in the plane of incidence (σ-polarisation) has been sent to the sample with the use of small mirror positioned in front of the cryostat window (Fig. 1a). The light emitted by the sample in the cone with the apex angle of 18° has been collected to the optical fibre with the use of lenses. Either σ- or π-component of luminescence has been selected by the analyser and the radiation

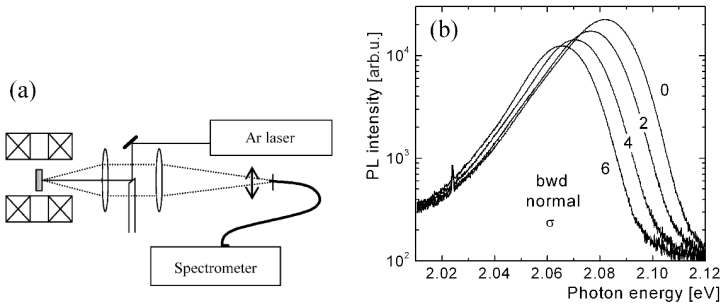

Fig. 1. (a) Experimental scheme and (b) PL spectrum of $Cd_{0.7}Mn_{0.3}Te$ crystals at the normal incidence of Ar laser light (the trace numbers show magnetic field values in [T]).

has been sent to a SPEX 0.33m monochromator (Fig. 1a). The spectrum has been recorded with a Jobin Yvon CCD array detector. The sample has been oriented so as to have its cleaved surface normal to the Ar laser beam or creating the angle of 45° to it. In the latter case the sample has been fixed to the bronze corner reflector (Fig. 2) allowing for measuring luminescence in the backward (bwd) direction relative to the incident beam or in the forward (fwd) one that actually coincided with the direction of Ar-laser beam specular reflection.

Two additional peaks of considerably less intensity have been observed at spectral intervals of 2.021–2.024 eV and at 2.0031–2.0038 eV. Their intensity and position did not depend on magnetic field. We guess that the origin of these lines could be Ar laser: relatively strong Ar lines being at 2.0087 eV and 2.0275 eV [26] are close to the observed ones although not identical with them. Let us note that Mueller and Gebhardt [12] have observed PL line at 2.023 eV in $Cd_{1-x}Mn_xTe$ under Ar^+-laser excitation (514.5 nm) but the line has been enormously broad (the full width at half maximum FWHM ≈ 100 meV). PL maximum at 2.02 eV has been observed elsewhere [6, 14] and assigned to different origins. We mention the sharp peaks to illustrate high accessible spectral resolution in our experiments. We retain four decimal numbers in the photon energy values leaving the possibility to round off when PL line is broad.

The main PL band shape (Fig. 1b, and Fig. 2) is asymmetric, inhomogeneously broadened and dependent on whether the light excitation (emission) isnormal or oblique. The red shift of PL maximum in magnetic field correlates

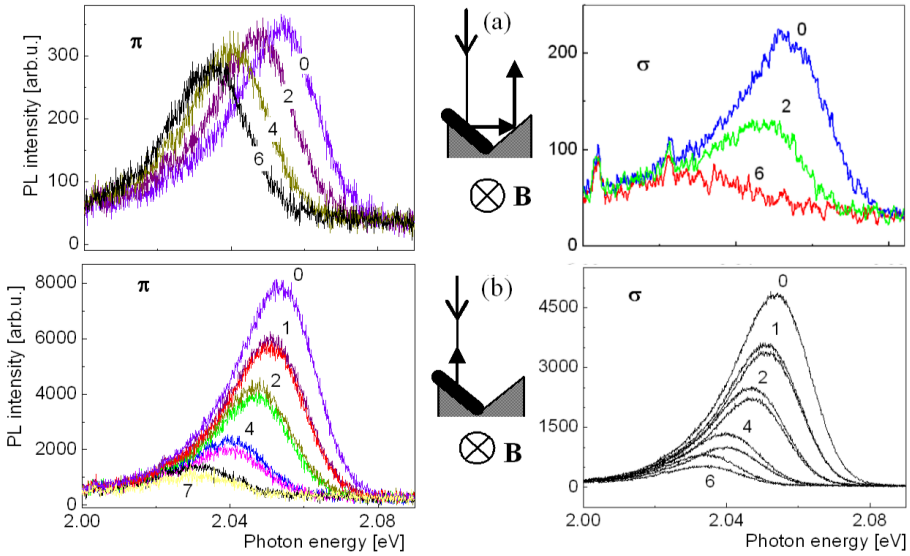

Fig. 2. PL spectrum of $Cd_{0.7}Mn_{0.3}Te$ crystals at the oblique incidence of Ar laser light for fwd (a) and bwd (b) directions, and for π and σ polarisation (the trace numbers show magnetic field values in [T]).

with the conventional model of Zeeman splitting (Fig. 3a) as will be discussed in the next sections.

3. Results

In the absence of magnetic field, PL maximum is seen to be at 2.0819 eV at the normal incidence, whereas in the oblique incidence case it is at 2.0536 eV (Fig. 3b). This significant offset becomes even more pronounced in high magnetic fields. The striking feature is that the PL maximum position is nearly the same both for π- and σ-polarisation (Fig. 3b). With the rise in magnetic field the main PL maximum moves to lower energy with the slightly different rate for bwd and fwd directions and light polarisation, although the approximate rate is 4 meV/T. Let us note that Hayes and co-workers [13] have reported the shift of PL maximum from 2.073 eV and $B = 0$ to 2.043 eV at $B = 8$ T in the same composition crystals at $T = 1.8$ K. These data fall between our upper and lower curves in Fig. 3. However, Hayes et al. did not specify light beam and magnetic field direction.

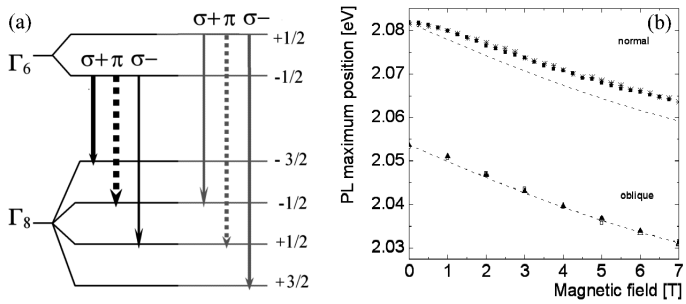

Fig. 3. Zeeman splitting scheme (a), and PL maximum position dependence on magnetic field in the normal and oblique incidence geometry in $Cd_{0.7}Mn_{0.3}Te$ crystals (b), dots — experiment, lines — modelling.

PL intensity exhibits essentially different behaviour in magnetic field in the oblique and normal geometry. In the oblique bwd geometry exponential decrease is observed): $I(B)/I(0) = \exp(-B/B_0)$, where the decay parameter B_0 is in the range of 2.27–2.77 T depending on polarisation (Fig. 4a). The same dependence is observed in the oblique fwd geometry for σ-component only (Fig. 4b), whereas π-component intensity exhibits nearly linear slow decrease in magnetic field. In the normal incidence geometry (Fig. 4c), the π-component intensity is nearly independent on magnetic field up to 7 T, whereas the σ-component intensity decreases 2 times attaining at highest magnetic fields the same level as that for the π-component. Maximum PL intensity in the normal incidence geometry is much higher than in the case of oblique incidence.

PL intensity is sensitive to magnetic field reversal. We refer to this effect as the non-reciprocity of luminescence and measure it by the ratio of PL intensities:

$[I(-B) - I(+B)]/[I(-B) + I(+B)]$. The non-reciprocity appears in backward emission both in σ- and π-polarisation; it ranges from 10 percent in the bwd π case to almost 60 percent in the bwd σ case at the oblique incidence.

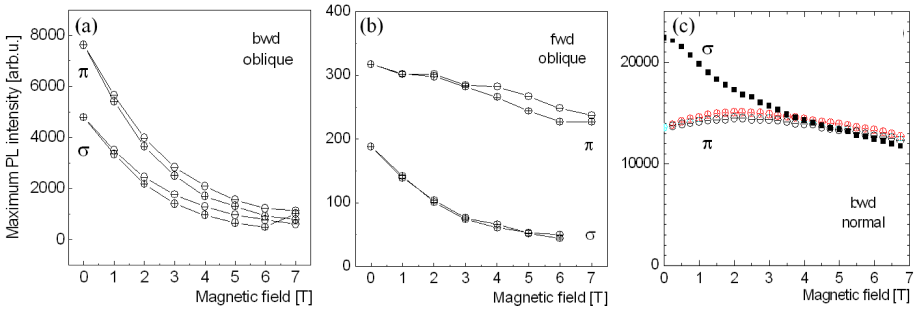

Fig. 4. Maximum PL intensity dependence on magnetic field in $Cd_{0.7}Mn_{0.3}Te$ crystals at the oblique incidence (a, b), and at normal incidence (c); circles with (+) and (–) signs show the effect of magnetic field reversal.

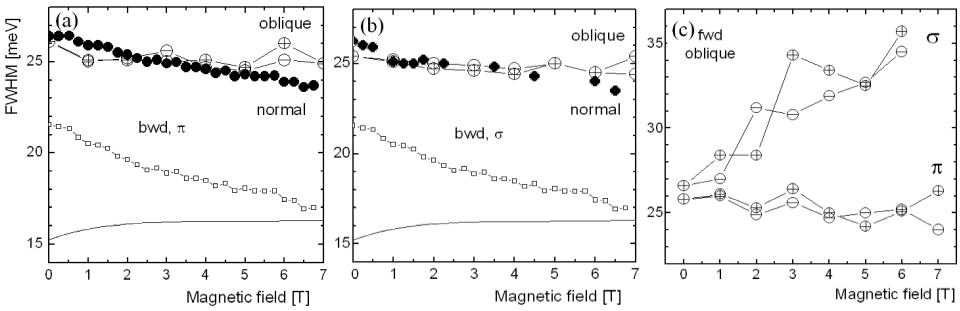

Fig. 5. FWHM of the main luminescence line as a function of magnetic field for the backward (a,b) and forward (c) emission in $Cd_{0.7}Mn_{0.3}Te$ crystals; circles with (+) and (–) signs show the effect of magnetic field reversal at the oblique incidence, and dots represent the normal incidence case. The lower curve in (a) and (b) represents the calculated alloy disorder contribution, and squares represent the estimated contribution of magnetisation fluctuation.

The full width at half maximum (FWHM) decreases with the rise of magnetic field in the normal incidence (emission) geometry, whereas it is rather constant (fluctuating between 25 and 28 meV) for the oblique bwd geometry (Fig. 5a,b). A considerable increase in FWHM is observed for the σ-component of forward emitted photons (Fig. 5c). Let us note that the inclined background baseline is subtracted when determining the FWHM values: the background band is thought to origin from other sources not readily related to free excitons. Without the background subtraction, PL line broadening at the oblique incidence is even more pronounced.

4. Discussion

We compare our experimental results with the existing models of exchange interaction of Mn^{2+} $3d^5$ and band (s,p) electrons. The $sp{-}d$ interaction manifests in the magnetic-field-induced splitting of the conduction and valence band edges [8, 27, 28]: $\Delta E_{\rm c} = -xN\alpha\langle S_z\rangle m_j$, $m_j = \pm 1/2$ and $\Delta E_{\rm v} = -xN\beta\langle S_z\rangle m_j$, $m_j = \pm 1/2, \pm 3/2$. Here N is the number of elementary cells per unit volume, α is the $s{-}d$ exchange integral for Γ_6-band electrons, β is the $p{-}d$ exchange integral for Γ_8 band holes, m_j is the magnetic quantum number, and $\langle S_z\rangle$ is the average component of the Mn^{2+} ion spin along the steady magnetic field $\boldsymbol{B}$. The $N\alpha$ and $N\beta$ values determined from experiments are –0.22 eV and 0.88 eV, respectively [4]. The conduction band at Γ_6 point splits into two sub-bands separated by $6|A_{\rm ex}|$ ($A_{\rm ex} = \frac{1}{6}xN\alpha\langle S_z\rangle$) and the valence band at Γ_8 point undergoes fourfold splitting related to light and heavy holes (Fig. 3a) resulting in four sub-bands situated equidistantly with the splitting of $2|B_{\rm ex}|$ ($B_{\rm ex} = \frac{1}{6}N\beta\langle S_z\rangle$) [3, 8, 27, 28]. The average spin of Mn site at $x = 0.3$ is $\langle S_z\rangle = S_0 B_{5/2}\{Sg_{\rm Mn}\mu_{\rm B}/[k_{\rm B}(T+T_0)]\}$ with the spin saturation value of $S_0 = 0.52$, and the characteristic temperature of $T_0 = 14.9$ K [3]. Here $B_{5/2}(x)$ is the Brillouin function for spin value of $S = 5/2$, $g_{\rm Mn} \approx 2$ is the effective Mn ion Lande factor, $\mu_{\rm B}$ is the Bohr magneton, $k_{\rm B}$ is the Boltzmann constant, and T is the temperature. According to the Zeeman splitting scheme (Fig. 3a), selection rules allow for 6 transitions between the sub-bands, however, our experimental results confirm the luminescence emission related only to the subset of the three lowest energy transitions. The change of effective band gap in magnetic field observed for the π component of emission is

$$E_{\rm g}(B) = E_{\rm g0} - 3|A_{\rm ex}| - |B_{\rm ex}|. \tag{1}$$

Taking the initial energy $E_{\rm g0}$ (at $B = 0$) as an adjustable parameter, we find that the experimental results on PL maximum shift towards lower energies in magnetic field, in very good agreement with the above discussed model for the oblique incidence (emission) (Fig. 3b). It is striking that the PL maximum position is independent of whether one observes the σ- or π-polarisation component of radiation, and we propose an explanation of this feature.

Symmetry relations for the wave vector $\boldsymbol{k}$, the electric vector $\boldsymbol{E}$, and the steady magnetic field $\boldsymbol{B}$, that are mutually transverse in the Voigt geometry, imply that the outgoing σ-polarisation light wave is linearly polarised. However, it is created by the σ^+ and σ^- transitions (Fig. 3a) being the sources of clockwise and anti-clockwise rotating electric fields. With the rise in magnetic field these two dipole-like sources emit at increasingly different frequencies, $\boldsymbol{E}_{\sigma^+} = \boldsymbol{E}_0\cos(\omega^+ t)$ and $\boldsymbol{E}_{\sigma^-} = \boldsymbol{E}_0\cos(\omega^- t)$. As a result of their interference, the σ-component of emission could be regarded as the wave packet propagating at the frequency of $(\omega^+ + \omega^-)/2$ with the amplitude modulated by the frequency of beats $\omega^+ - \omega^-$. As far as the partial frequencies are

$$\omega^+ = \frac{1}{\hbar}(E_{g0} - 3|A_{ex}| - 3|B_{ex}|), \quad \text{and} \quad \omega^- = \frac{1}{\hbar}(E_{g0} - 3|A_{ex}| + |B_{ex}|), \quad (2)$$

the result of superposition should be $\omega = (\omega^+ + \omega^-)/2 = (E_{g0} - 3|A_{ex}| - |B_{ex}|)/\hbar$, i.e., the apparent energy of photons of the σ-polarisation in the Voigt geometry is the same as that for the π-polarisation (Eq. (1)). This is observed experimentally (Fig. 3b). In contrast to the case of oblique incidence, the normal incidence (emission) exhibits increasing deviation from the conventional model with the rise in magnetic field (Fig. 3). This discrepancy, as well as the observed different PL maximum position (2.082 eV at $\varphi = 0$ and 2.053 eV at $\varphi = 45°$) is the feature that was not previously reported.

In our PL line shape analysis we focus first on the line broadening due to alloy disorder which gives rise to spatial fluctuation of potential (band-gap). Following Schubert et al., we assume the random distribution of cations (Cd, Mn) allowing us to describe the probability of finding n Mn atoms in any group-II site by the binomial (Bernoulli) distribution [29]:

$$P(n) = \left[\begin{array}{c} KV \\ n \end{array} \right] x^n (1-x)^{KV-n}. \quad (3)$$

Here K is the density of cations in the crystal, $K = 4a_0^{-3}$. For the $Cd_{0.7}Mn_{0.3}Te$ crystals the lattice constant value is $a_0 = 6.43$ Å [8]. The number of cation sites in the exitonic volume is determined as KV_{exc}, and the exitonic volume is calculated using the hydrogen model $V_{exc} = 4\pi r_{exc}^3/3$, with the radius of $r_{exc} = (\varepsilon_{st} a_B)/m_r$. Here $m_r = (m_e^{-1} + m_{hh}^{-1})^{-1}$ is the exiton reduced mass, m_e, m_{hh} are the electron and heavy hole effective masses ($m_e = 0.096 m_0$ [30] and $m_{hh} = 0.81 m_0$ [31]), and the static dielectric constant is $\varepsilon_{st} = 10.2$ [32]. The numerical values taken for CdTe give $r_{exc} \approx 6.3$ nm. The standard deviation of alloy composition and the band-gap energy given by the binomial distribution are [29]:

$$\sigma_x = [x(1-x)/KV_{exc}]^{1/2}, \quad \text{and} \quad \sigma_E = (\mathrm{d}E_g/\mathrm{d}x)\sigma_x, \quad (4)$$

and the FWHM is equal to $2.36\sigma_E$. Taking the value of $\mathrm{d}E_g/\mathrm{d}x = 1.59$ that is the difference of the band-gap energies of CdTe and MnTe crystals [8] we find for $x = 0.3$ the FWHM value to be 13.6 meV. It is approximately half of the experimentally observed linewidth. As the second step, we seek for the value of $\mathrm{d}E_g/\mathrm{d}x$ at $x = 0.3$ as a function of magnetic field. For this purpose we have used E_g measured in exitonic reflection experiments for the set of composition $0.005 \leq x \leq 0.3$ in magnetic field varying up to 6 T [2]. From these data we have constructed the matrix of $E_g(x, B)$ allowing to determine the function of $\mathrm{d}E_g/\mathrm{d}x = f(B)$. Combining it with Eq. (4), the alloy-related FWHM value reveals the tendency to increase (Fig. 5a,b). We interpret this increase as the enhancement of alloy-disorder-related potential profile contrast in magnetic fields.

The FWHM narrowing with the rise in magnetic field is related to settling down magnetic fluctuations. We determine this contribution from the

alloy-disorder contribution and the experimental linewidth: $\mathrm{FWHM_{magn}} = (\mathrm{FWHM^2_{exper}} - \mathrm{FWHM^2_{alloy}})^{1/2}$. It decreases with the rise in magnetic fields a little bit more rapidly than the total FWHM (Fig. 5, squares). Having in mind that the $\mathrm{FWHM_{magn}}$ changes as $\lambda_{\mathrm{M}}^{2/3}$, where λ_{M} is the mean linear size of magnetic fluctuation [19, 20], we estimate the mean size of "magnetic quantum dots" in the crystal matrix to be about 2.5 nm, i.e., nearly 1/5 of the heavy-hole free-exciton diameter.

The FWHM increase with magnetic field that observed for the σ-polarisation in the oblique forward emission geometry (Fig. 5c) does not fit with the existing models of alloy disorder and magnetisation fluctuations. The broadening can result from an overlap of red-shifted main PL band with the emission band of deeper levels.

Returning to the question on the origins of the large difference in maximum PL positions observed at normal and oblique incidence, we relate it to the non-zero in-plane wave vector rendered by Ar-laser photons to excitons (actually to exciton--polaritons). At the incidence angle of 45° the in-plane wave vector component is $k_{||} = 9.1 \times 10^4$ cm^{-1}. It exceeds the corresponding value of lower-energy photons emitted in the direction of specular reflection. Therefore the radiative recombination of excitons needs to be accompanied by the emission of other quasiparticles taking the excess momentum. The latter is small, therefore the quasiparticles involved could be, e.g., either the Brillouin-zone-centre optical phonons or the sum of two nearly opposite large-momentum phonons. A phonon energy spectrum is not exactly known in the temperature range of our experiments but one can extrapolate the data reported in [24]. For the optical phonon modes in $Cd_{0.7}Mn_{0.3}Te$ at the Brillouin zone centre the extrapolated values are 18, 20, 24, and 25 meV. The highest phonon energy is near to but still less than the PL maximum off-set at $B = 0$. If excitons couple to light waves then one can think on the resulting polariton accumulation at the bottleneck region of lower dispersion branches (Fig. 6). These polaritons emit lower-energy photons and require phonon assistance in ac-

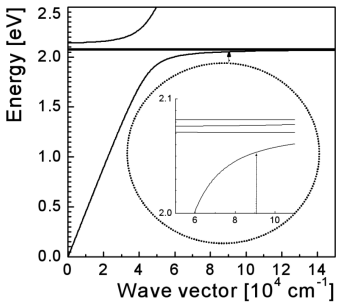

Fig. 6. Dispersion branches of polaritons calculated with an account for two excitonic oscillators with the characteristic energy of 2.082 eV and 2.061 eV, and the background dielectric constant is $\varepsilon = 7.1$. The inset shows a magnified region where polariton accumulation and the lower-energy photon emission at oblique angle are feasible.

cessing the region. This could explain much lower PL intensity observed in the case of oblique emission as compared to the case of normal one, as well as the exponential decrease in PL intensity with the rise in magnetic field. In order to account for the signature of PL line broadening due to excitons pinned to magnetic quantum dots we have included in the dispersion modelling two excitons differing in energy by 1 percent. As a result, an additional branch has arisen anticrossing with the lower one (Fig. 6). Polariton accumulation in this band seems to be especially favourable due to the high density of states.

5. Conclusion

This experimental research on photoluminescence from the cleaved surface of $Cd_{1-x}Mn_xTe$ crystals has shown that the PL spectral range, intensity, polarisation, and linewidth characteristics in magnetic field are essentially different depending on whether the light excitation and emission is normal to the surface or oblique to it. Therefore a precise control of the angular geometry is needed when applying photoluminescence as the conventional method of DMS characterisation. This survey challenges for further experiments on DMS micro-luminescence with high spatial and angular resolution, e.g., using recently published method applied for detecting polariton condensation [33]. On the other hand, $Cd_{1-x}Mn_xTe$ crystal boundary presents a barrier localising light waves at the surface plane, whereas the random potential profiles of alloy- and magnetisation fluctuations restrict lateral motion of exciton polaritons. Assuming the mean depth of random potential wells to be *ca.* 25 meV (experimental FWHM) one can think about the crystal as a disordered mosaic of nanometre-scale magnetic quantum dots. This seems to be a natural playground for magnetically controlled nanophotonics.

Acknowledgments

The work has been partially supported by the EU Centre of Excellence in PRAMA project and by the National Science Foundation of Lithuania project V-05095.

References

[1] N.T. Khoj, J.A. Gaj, *Phys. Status Solidi B* **83**, K133 (1977).

[2] J.A. Gaj, P. Byszewski, M. Cieplak, G. Fishman, R.R. Galazka, J. Ginter, M. Nawrocki, N.T. Khoi, R. Planel, R. Ranvaud, in: *Physics of Semiconductors, 14th Inter. Conf. Phys. Semicond., Edinburgh 1978*, Conf. series No. 43, Ed. B.L.H. Wilson, The Institute of Physics, Bristol 1978, p. 1113.

[3] J.A. Gaj, R. Planel, G. Fishman, *Solid State Commun.* **29**, 435 (1979).

[4] A. Twardowski, M. Nawrocki, J. Ginter, *Phys. Status Solidi B* **96**, 497 (1979).

[5] R.R. Galazka, Shoichi Nagata, P.H. Keesom, *Phys. Rev. B* **22**, 3344 (1980).

[6] M.P. Vecchi, W. Giriat, L. Videla, *Appl. Phys. Lett.* **38**, 99 (1981).

[7] D.U. Bartholomew, J.K. Furdyna, A.K. Ramdas, *Phys. Rev. B* **34**, 6943 (1986).

[8] J.K. Furdyna, *J. Appl. Phys.* **64**, R29 (1988); O. Goede, W. Heimbrodt, *Phys. Status Solidi B* **146**, 11 (1988).

[9] Eunusson Oh, D.U. Bartholomew, A.K. Ramdas, *Phys. Rev. B* **44**, 10551 (1991).

[10] Eunusson Oh, A.K. Ramdas, J.K. Furdyna, *J. Lumin.* **52**, 183 (1992).

[11] W. Gebhardt, V. Gebhardt, E. Mueller, F. Wuensh, W.M. Becker, *J. Lumin.* **24/25**, 731 (1981).

[12] E. Mueller, W. Gebhardt, *Phys. Status Solidi B* **137**, 259 (1986).

[13] W. Hayes, K.S. Wong, J.F. Ryan, A.K. Ramdas, *J. Lumin.* **40/41**, 72 (1988).

[14] Y.R. Lee, A.K. Ramdas, R.L. Aggarwal, *Phys. Rev. B* **38**, 10600 (1988).

[15] M.M. Moriwaki, W.M. Becker, W. Gebhardt, R.R. Galazka, *Phys. Rev. B* **26**, 3165 (1982).

[16] J.M. Fatah, T. Piorek, P. Harrison, T. Stirner, W.E. Hogston, *Phys. Rev. B* **49**, 10341 (1994).

[17] S. Lee, M. Dobrowolska, J.K. Furdyna, H. Huo, L.R. Ram-Mohan, *Phys. Rev. B* **54**, 16939 (1996).

[18] Su-Huai Wei, A. Zunger, *Phys. Rev. B* **35**, 2340 (1987).

[19] T. Dietl, *J. Magn. Magn. Mater.* **38**, 34 (1983).

[20] R. Brazis, J. Kossut, *Solid State Commun.* **122**, 73 (2002).

[21] W.M. Becker, R. Bylsma, M.M. Moriwaki, R.Y. Tao, J.W. Richardson, *Solid State Commun.* **49**, 245 (1984).

[22] M.I. Kaganov, A.P. Levanyuk, S.A. Minyukov, A.V. Chubukov, in: *Nonlinear Surface Electromagnetic Phenomena*, Eds. H.E. Ponath, G.I. Stegeman, North Holland, Amsterdam 1991, p. 497.

[23] R. Huang, Y. Yamamoto, R. André, J. Bleuse, M. Muller, H. Ulmer-Tuffigo, *Phys. Rev. B* **65**, 165314 (2002).

[24] S. Venugopalan, A. Petrou, R.R. Galazka, A.K. Ramdas, S. Rodriguez, *Phys. Rev. B* **25**, 2681 (1982).

[25] F. Nizzoli, D.L. Mills, in: *Nonlinear Surface Electromagnetic Phenomena*, Eds. H.E. Ponath, G.I. Stegeman, North Holland, Amsterdam 1991, p. 445.

[26] Strong Lines of Argon: http://physics.nist.gov./PhysRefData/Handbook/Tables/argontable2_a.htm .

[27] J.A. Gaj, J. Ginter, R.R. Galazka, *Phys. Status Solidi B* **89**, 655 (1978).

[28] N. Brandt, V. Moshchalkov, *Adv. Phys.* **33**, 193 (1984).

[29] E.F. Schubert, E.O. Gobel, Y. Horikoshi, K. Ploog, H.J. Queisser, *Phys. Rev. B* **30**, 813 (1984).

[30] K.K. Kanazawa, F.C. Brown, *Phys. Rev.* **135**, A1757 (1964).

[31] R. Romestain, C. Weisbuch, *Phys. Rev. Lett.* **45**, 2067 (1980).

[32] S. Perkowitz, R.H. Torland, *Phys. Rev. B* **9**, 545 (1974).

[33] M. Richard, J. Kasprzak, R. Romestain, R. André, Le Si Dang, *Phys. Rev. Lett.* **94**, 187401 (2005).